Results in Engineering 16 (2022) 100713

Contents lists available at ScienceDirect

Results in Engineering

journal homepage: www.sciencedirect.com/journal/results-in-engineering

Performance enhancement of cementitious soil stabilizers using incorporated nanosilica

Ebrahim Najafi Kani [a], Amir Hossein Rafiean [b], Mohsen Tavakolzadeh [a], Seyed Hamidreza Ghaffar [c,d,*]

[a] Faculty of Chemical, Petroleum, and Gas Engineering, Semnan University, Semnan, 35195-363, Iran
[b] Faculty of Civil Engineering, Semnan University, Semnan, 35195-363, Iran
[c] Department of Civil and Environmental Engineering, Brunel University London, Uxbridge, UB8 3PH, United Kingdom
[d] Applied Science Research Center, Applied Science Private University, Jordan

ARTICLE INFO

Keywords:
Soil stabilization
Nanosilica
Portland cement
Phosphorus slag
Alkali-activated slag

ABSTRACT

This investigation aims to study the performance of different hybrid binders as environmentally-friendly cementitious soil stabilizers as well as Nanosilica as a reactive powder. Mechanical properties and microstructural analysis in addition to the molecular and mineralogical specifications were investigated to evaluate the performance of stabilized soil samples. For this purpose, a series of experimental tests including scanning electron microscopy (SEM), Fourier-transform infrared spectroscopy (FTIR), and X-ray diffraction (XRD) are considered as well as mechanical tests to investigate the various aspects of the material. The results showed that the incorporation of Nanosilica not only improved the unconfined compressive strength (UCS) of the stabilized samples, but also the elastic modulus which is indicative of Nanosilica's tendency to increase the ductility of samples. In Portland cement (PC) and phosphorus slag blended cement (SBC)-based samples, the results confirmed that samples containing Nanosilica possess an intensified C–S–H phase compared to other samples. It appeared that the supplied reactive Nanosilica to the matrix showed better participation reaction of Ca2+ of Portlandite for formation of extra C–S–H phase due to the observed phase change of needle-like crystals of Portlandite in lower amount with smaller particles. Moreover, the microstructure results revealed that the presence of Nanosilica leads to more densified binder matrix with more coverage of soil particles. The incorporation of Nanosilica in SBC exhibited a more densified matrix with higher UCS values compared to PC samples. The presence of 2 wt% of Nanosilica in the alkali-activated phosphorus slag cement (AAC)-based samples resulted in lengthening the aluminosilicate chain with more substituted Al with reactive Si. In AAC-based samples, with incorporated Nanosilica a compact interfacial bond of matrix and soil particles was observed.

1. Introduction

Cement is one of the primary construction materials that provides many benefits for developing infrastructure due to its high efficiency with reasonable costs. However, this material has its own drawbacks which are thoroughly investigated during recent years, such as greenhouse gas emissions, energy consumptions, and brittleness [1]. Cement plays a critical role in chemical soil stabilization where the engineering properties of the soil are improved in poor quality grounds. The role of cement is to provide a strong bond structure between soil particles through chemical reactions so that a reliable base for engineers to build on is prepared [2,3]. Stabilized soil by different binders consist of artificially stable structure with mixture of cementitious bonds coating soil particles named soil-binder matrix. Many attempts have been made to use an environmentally-friendly alternative to conventional Portland cement. Different types of industrial by-products and wastes have been developed with an acceptable performance in engineering application which improves the sustainability credentials of the construction projects [2,4–7]. Phosphorus slag, similar to blast furnace slag is an amorphous by-product of phosphoric acid production (dry method production process) and its main chemical components consists of calcium oxide and silicon oxide. In the production process, the raw

* Corresponding author. Department of Civil and Environmental Engineering, Brunel University London, Uxbridge, UB8 3PH, United Kingdom.
E-mail addresses: e_najafi@semnan.ac.ir (E.N. Kani), A.h.rafiean@gmail.com (A.H. Rafiean), mohsent778@gmail.com (M. Tavakolzadeh), seyed.ghaffar@brunel.ac.uk (S.H. Ghaffar).

https://doi.org/10.1016/j.rineng.2022.100713
Received 13 September 2022; Received in revised form 15 October 2022; Accepted 17 October 2022
Available online 21 October 2022

materials which consist of phosphorous ore and coke are sintered at the temperature of 1400 °C in an electric furnace to be melted and then the remained melt by-product is quenched in water to develop the granular phosphorous slag [8–10]. One of the most beneficial alternatives to Portland cement (PC) is blended cements, i.e., hydraulic cements consisting of a homogeneous blend of cement and other supplementary cementitious materials (SCM). Some known and well-experienced SCMs could either be industrial by-products or other wastes, like blast furnace slag, fly ash, silica fume, and so on [11]. Another alternative to PC is alkali-activated cements (AAC), which is mainly produced by two parts, one part is source material and the other part is alkali activator which activates the first part to produce a binder. Researchers have used various materials like abovementioned SCM's to produce a durable AAC [7,12].

Various nanomaterials have recently been used to improve the properties of cementitious binders [13–17]. Among the used nanomaterials, Nanosilica can be considered as the most popular one due to its high specific surface area, which can interact dynamically with soil constituents and thus have significant influence on microstructure and mechanical properties of stabilized soil by filling pores of matrix, strengthening the interfacial transition zone (ITZ), and enhancing distribution of hydration products through nucleation effect [18,19]. Additionally, it can increase the pozzolanic reactions and may promote the stiffness of soil skeleton matrix. Nanosilica consumes calcium hydroxide ($Ca(OH)_2$), which arrays in the ITZ between hardened cement paste and soil particles. Additionally, Nanosilica enhances the production step of hydrated calcium silicate (C–S–H) which increases the strength of the hardened cement composites [20,21]. Reduction of carbon dioxides emission and environmental impact has been main concern of researchers during past decades, however, technical performance of blended cements and alkali-activated materials, as the most common alternatives to OPC, have to be considered and compared. Therefore, the performance of different cementitious composites for soil stabilization in terms of mechanical and microstructure properties have been investigated. The effect of Nanosilica incorporation is also investigated for each binders separately. Comparing different categories of chemical stabilizers based on phosphorus slag, i.e. SBC and AAC, by comparing with OPC as a conventional soil stabilizer, and evaluating the effect of Nanosilica on each of stabilizers is the novelty of this research. Moreover, analysis, such as, scanning electron microscopy (SEM), Fourier-transform infrared spectroscopy (FTIR), and X-ray diffraction (XRD) are assisted to reveal the molecular and mineralogical aspects of the pastes itself. The effects of type of binder, incorporation of Nanosilica in each binder, and curing time on mechanical properties of stabilized soil are the main parameters being studied. The findings provide significance for practical usage of cementitious materials in using phosphorus slag and Nanosilica.

2. Materials and methods

2.1. Raw materials

The soil is provided from shoreline of Caspian Sea, in the north of Iran. According to unified soil classification system (USCS), this soil is classified as poorly graded sandy soil (SP) with specific gravity of 2.7. The soil is pure sand with a uniformity and curvature coefficient of 1.15 and 0.99, respectively. The minimum and maximum unit weight are 14.72 and 17.67, respectively. Physical properties of the used soil is presented in Table 1. Fig. 1 presents the scanning electron microscopy (SEM) images and elemental analysis (EDS) of sandy soil grains with the magnitude of 100×. Table 2 shows the EDS results done at the selected part shown on Fig. 1.

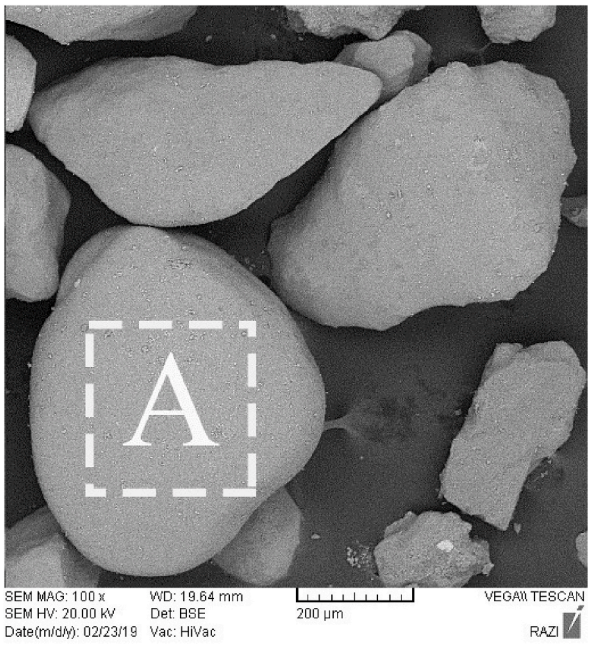

Fig. 1. SEM images of soil (in magnification of 100x).

The PC, (CEM I 42.5R) with Blaine specific area of 350 ± 0.5 m^2/kg is operated as the control sample. The phosphorus slag as a raw material for producing phosphorus slag-blended cement and alkali-activated phosphorus slag cements is considered. Chemical analysis of the PC and phosphorus slag are presented in Table 3. The granular phosphorus slag is grounded to a Blaine specific surface area of 350 ± 0.5 m^2/kg, similar to OPC. A laboratory mill (110 mm radius and 380 mm length) was used for this purpose. Based on laser particle size analyzer, the mean particle diameter of the PC and phosphorus slag are 11.38 μm and 13.18 μm, respectively. Figs. 2 and 3 present the SEM images of PC and phosphorus slag powders with the magnitude of 1000x and 5000x, respectively.

Tables 4 and 5 present the EDS results done on the selected part shown on images in Figs. 2 and 3.

Fig. 4 shows the X-ray diffraction (XRD) pattern of phosphorus slag. In the amorphous structure of phosphorus slag, a small amount of crystalline magnesium oxide (MgO, JCPDS 02–1207) can be seen.

Sodium silicate (Na_2SiO_3; 32.87 wt% of SiO_2, 24.21 wt% of Na_2O, and 42.92 wt% of H_2O) and sodium hydroxide (NaOH, 99 wt% purity) are provided for producing the alkaline activator solution. SiO_2 nanoparticles, (99.5 wt% purity) is supplied from US research nano-materials Inc., Houston, USA. Properties of the used Nanosilica is shown in

Table 2
Results of Elemental Analysis on Point A shown in Fig. 1

Element (wt. %)	O	Mg	Al	Si	S	K	Ca	Fe
	47.91	2.18	0.87	2.54	2.47	0.19	42.52	1.33

Table 1
Properties of soil.

	Specific gravity, Gs	Minimum unit weight, γmin (kN/m3)	Maximum unit weight, γmax (kN/m3)	D10 (mm)	D30 (mm)	D60 (mm)	The coefficient of curvature, *Cc*	The coefficient of uniformity, Cu
Soil	2.7	14.72	17.67	0.15	0.16	0.17	0.99	1.15

Table 3
Chemical analysis of the used materials (wt.% determined by X-ray fluorescence method).

Component	SiO_2	Al_2O_3	Fe_2O_3	CaO	MgO	P_2O_5	K_2O	Na_2O
Portland Cement	21.99	4.31	4.15	62.88	2.86	–	0.47	0.21
Phosphorus slag	38.39	7.66	0.90	45.16	2.60	1.50	0.56	0.43

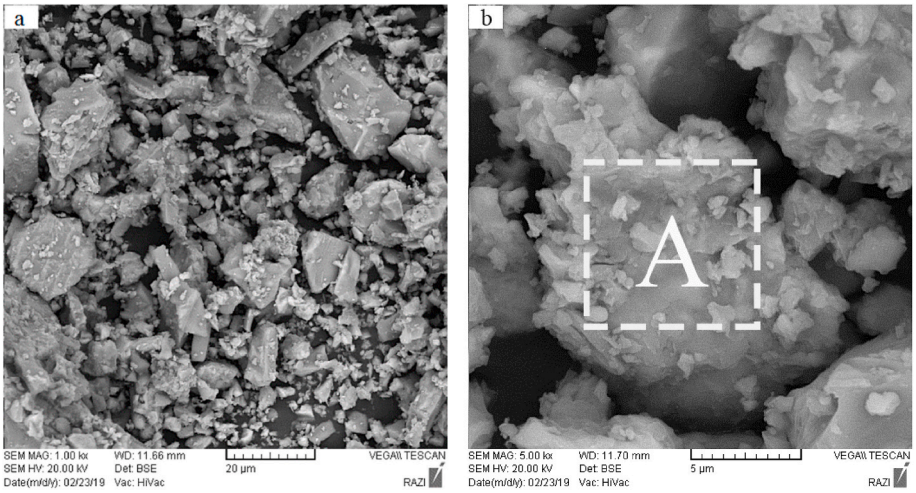

Fig. 2. SEM of PC in magnification of (a) 1000x, and (b) 5000x

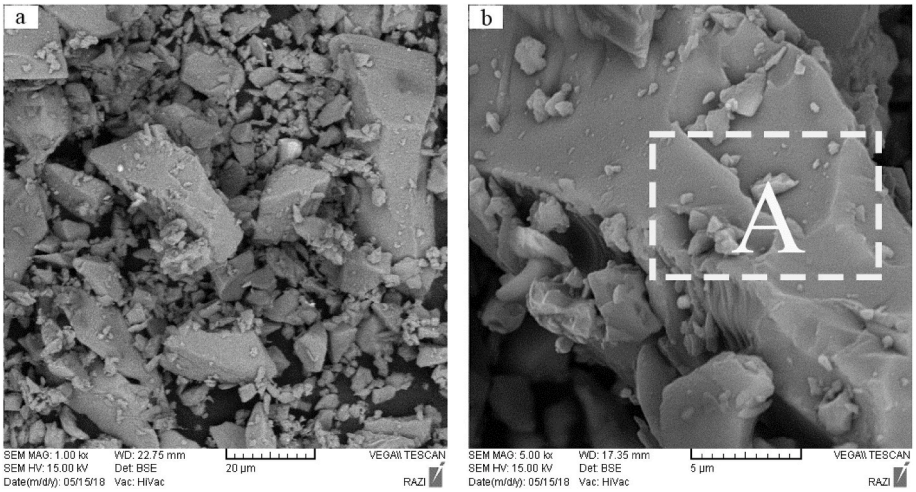

Fig. 3. SEM of phosphorus slag in magnification of (a) 1000x, and (b) 5000x

Table 4
Results of elemental analysis on point A shown in Fig. 2

Element (wt.%)	O	Mg	Al	Si	Ca	Ti	Fe
	26.61	0.52	19.48	2.65	32.97	2.09	15.69

Table 5
Results of elemental analysis on Point A shown in Fig. 3

Element (wt.%)	O	Mg	Al	Si	S	K	Ca
	37.84	0.29	2.51	15.60	4.19	0.71	38.87

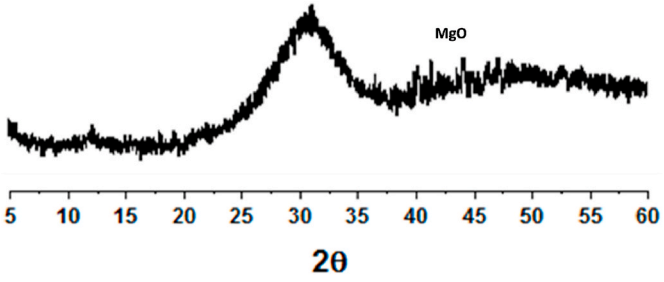

Fig. 4. X-ray diffraction data for phosphorus slag.

Table 6
Physical properties of nanosilica.

Properties	APS (nm)	SSA (cm^2/g)	Bulk Density (g/cm^3)	True Density (g/cm^3)	Shape	Purity
Nanosilica	20–30	180–600	<0.1	2.4	White Powder	>99%

Table 6.

2.2. Sample preparation

Three different kinds of binders are used to stabilize soil, i.e. PC, SBC, and AAC. SBC is produced by mixing PC and ground phosphorus slag with the proportion of 7:3 in the used laboratory mill for 10 min to be homogenized well. The selected proportion was considered based on some trial and error tests which resulted better and acceptable mechanical performance compared to other proportions. Table 7 shows the produced paste identification and related composition. For preparing AAC binder, at first the activator solution is prepared and then added to the ground phosphorus slag. The activator is prepared by adding sodium hydroxide to water to be dissolved, and then the determined amount of sodium silicate is added to the solution. Amount of sodium hydroxide and sodium silicate are so determined that 18 wt% of Na_2O for the used slag are supplied with the regulated SiO_2/Na_2O mass ratio of 0.2. In the other word, sodium hydroxide is supplying Na_2O component and sodium silicate is supplying SiO_2 and silica component. This composition for the produced activator will be adjusted in the pure paste and in the combination of paste with the soil. The total used amount of water for all of the prepared pastes are considered based on water/solid ratio of 0.4. The total water, here, is the combination of the introduced water from sodium silicate plus the required water to achieve the considered water/solid ratio.

For mixtures that contain Nanosilica, the nanomaterial is blended at determined percentages of 2, 4, and 6 wt% with solid material and homogenized all types of binders in a mechanical stirrer.

The binders are combined to the soil until a uniform blend is achieved. The added binders are determined a constant usage amount of 7 wt% of dry soil. For this purpose, each of the binders of PC, SBC, and AAC added to the wetted soil and then mixing procedure started for 10 min in a rotary mixing machine. Then by tamping and compressing the treated soil, final stabilized soil samples are produced. The mixtures were casted into the split mould with three equal layers to achieve the relative density of 55%, based on weight-volume relationships. The water-to-total solid ratio (W/S) of all stabilized soil samples is designed as 18 wt%. Samples are removed from their mould after considered curing time in moist room to be ready for mechanical experimental tests. The used mould is 80 mm in height and 40 mm in diameter in case of UCS test.

Table 7
Summary of the binder composition.

Paste Series Identification	Paste Name	Series details	Mixture ratio
I	PC	PC Powder (PCP) + Water	W/PCP = 0.4
II	SBC	30% Phosphorus Slag Powder (PSP) + 70% PC Powder (PCP) + Water	PSP/PCP = 0.43 W/Solid material = 0.4
III	AAC	Phosphorus Slag Powder (PSP) + Alkali Activator (AA) (Sodium Hydroxide (SH) and Sodium Silicate (SS)) + Water	SS/SH = 0.46 AA/PSP = 0.3 W/Solid material = 0.4

2.3. Testing methods

The prepared stabilized soil specimens are cured in an atmosphere of 95% relative humidity at 25 °C for 28 and 90 days. Before UCS test, the sample dimensions are measured with a digital caliper. The diameter and height of each sample are measured in three different points. UCS test according to ASTM D2166 are conducted in the apparatus with a constant vertical load rate of 1 mm/min for each mix, three identical specimens are used in the same curing time and the average of three values are considered as the reported strength value. Failure strain values are presented for investigating the failure mechanism of samples. Table 8 shows the composition of the stabilized soil samples used for UCS test.

Scanning electron microscopy along with SEM/EDS was conducted for samples listed in Table 9 using VEGA\TESCAN-LMU to investigate their microstructure. The broken fragments of 90-day-cured specimens of UCS tests samples were chosen to be golden coated before SEM test.

X-ray diffraction (XRD) is implemented for studying crystalline phases of some PC- and SBC- based samples after 90-days of curing, i.e. P7C, P7C6N, P7BC, and P7BC6N. The XRD test is carried out by Bruker D8 ADVANCE at the range of 10–60° with a scanning rate of 3.9°/min. Deliverance, an anti-scatter, and receiving slit of this test are all 1. FTIR test was conducted to study the effect of Nanosilica in AAC specimens on molecular structure of binders for P7G, P7G2N, and P7G6N samples. This test is performed by Shimadzu-8400S by using standard KBr technique, then the FTIR spectra are collected in transmittance mode from 400 to 4000 cm^{-1} with a sensitivity of 4 cm^{-1} and 64 scans per spectrum. Table 10 illustrates the composition of the binders samples used for XRD and FTIR test.

3. Results and discussion

3.1. Unconfined compressive strength

Fig. 5 represents the results of UCS test for stabilized soil samples. As seen, adding Nanosilica to PC- and SBC-based stabilized soil samples could be the cause of an increase in the UCS values. The trend of UCS values for AAC-based samples seems to be different, although adding Nanosilica to AAC-based stabilized soil could generally improve the UCS values of samples. The UCS values are decreased by increasing the percentage of Nanosilica from 2 to 6 wt% of binder (P7G2N > P7G4N > P7G6N > P7G). Improvement of PC-based stabilized soil samples in

Table 8
Summary of the UCS test stabilized soil samples composition.

Sample Name	Binder Percentage (%)	Nanosilica Percentage (%)	Description
P7C	7	0	SP + 7% of PC
P7C2N		2	SP + 7% of PC+ 2% of Nanosilica
P7C4N		4	SP + 7% of PC+ 4% of Nanosilica
P7C6N		6	SP + 7% of PC+ 6% of Nanosilica
P7BC	7	0	SP + 7% of SBC
P7BC2N		2	SP + 7% of SBC + 2% of Nanosilica
P7BC4N		4	SP + 7% of SBC+ 4% of Nanosilica
P7BC6N		6	SP + 7% of SBC+ 6% of Nanosilica
P7G	7	0	SP + 7% of AAC
P7G2N		2	SP + 7% of AAC+ 2% of Nanosilica
P7G4N		4	SP + 7% of AAC+ 4% of Nanosilica
P7G6N		6	SP + 7% of AAC+ 6% of Nanosilica

Table 9
Summary of the SEM/EDS test Samples composition.

Sample Name	Binder Percentage (%)	Nanosilica Percentage (%)	Description
P7C	7	0	SP + 7% of PC
P7C6N		6	SP + 7% of PC+ 6% of Nanosilica
P7BC	7	0	SP + 7% of SBC
P7BC6N		6	SP + 7% of SBC+ 6% of Nanosilica
P7G	7	0	SP + 7% of AAC
P7G2N		2	SP + 7% of AAC+ 2% of Nanosilica
P7G6N		6	SP + 7% of AAC+ 6% of Nanosilica

Table 10
Summary of the XRD and FTIR tests Samples composition.

Sample Name	Test type	Nanosilica Percentage (%)	Binder Composition
C0N	XRD	0	PC
C6N		6	PC+ 6% of Nanosilica
BC0N		0	SBC
BC6N		6	SBC+ 6% of Nanosilica
AAC0N	FTIR	0	AAC
AAC2N		2	AAC+ 2% of Nanosilica

presence of Nanosilica are greater compared to the similar SBC-based ones, however, P7BC samples has a greater UCS values compared to P7C samples. Moreover, AAC-based samples (P7G) show quite higher compressive strength than PC-based samples (P7C), i.e. 0.73 MPa for P7G, and 0.33 MPa for P7C after 90 days of curing. This trend is also observed for 28 days cured samples. An increase of Nanosilica to 2, 4, and 6 wt% after 90 days of curing improve the UCS value of PC-based stabilized soil by about 297, 339, and 336% compared to no added Nanosilica.

By adding Nanosilica, the UCS value of stabilized soil by PC is increased from 0.33 MPa for P7C to 1.44 MPa for P7C6N, after 90 days of curing. It is evident from Fig. 5 (a) (b), P7C4N and P7C6N approximately possess the same UCS value, which indicates that adding more than 4 wt% Nanosilica has no effect on UCS improvement of PC-based samples.

Adding Nanosilica to SBC paste showed steady increase in strength by increase in usage amount of Nanosilica after 28 days (P7BC: 0.76, P7BC2N: 0.81, P7BC4N: 0.89, and P7BC6N: 1.10 MPa), but there is a slight change on UCS value after 90 days by increasing the percentage of Nanosilica (P7BC: 0.88, P7BC2N: 0.89, P7BC4N: 0.99, and P7BC6N: 1.23 MPa). It could be concluded that added Nanosilica is more beneficial in short term than long term approach in terms of mechanical strength. An increase of Nanosilica to 2, 4, and 6 wt% after 90 days of curing improve the UCS value of SBC-based stabilized soil by about 1.14, 12.5, and 39.77% compared to no added Nanosilica. The acceleration effect of Nanosilica in cement and blended cement is well reported in the literature, the essential role of Nanosilica is its participation in the hydration and working as nucleation site for precipitation of C–S–H gel. Additionally, its chemical reactivity and its contribution in pozzolanic reaction due to the high surface area could be the second reason of its successful effect on cement and blended cement matrix [22–25].

In stabilized soil samples by AAC, adding Nanosilica shows an increase on UCS values, which is improved from 0.73 MPa to 1.76 MPa for P7G and P7G2N, respectively. However, UCS values show a sharp fall by

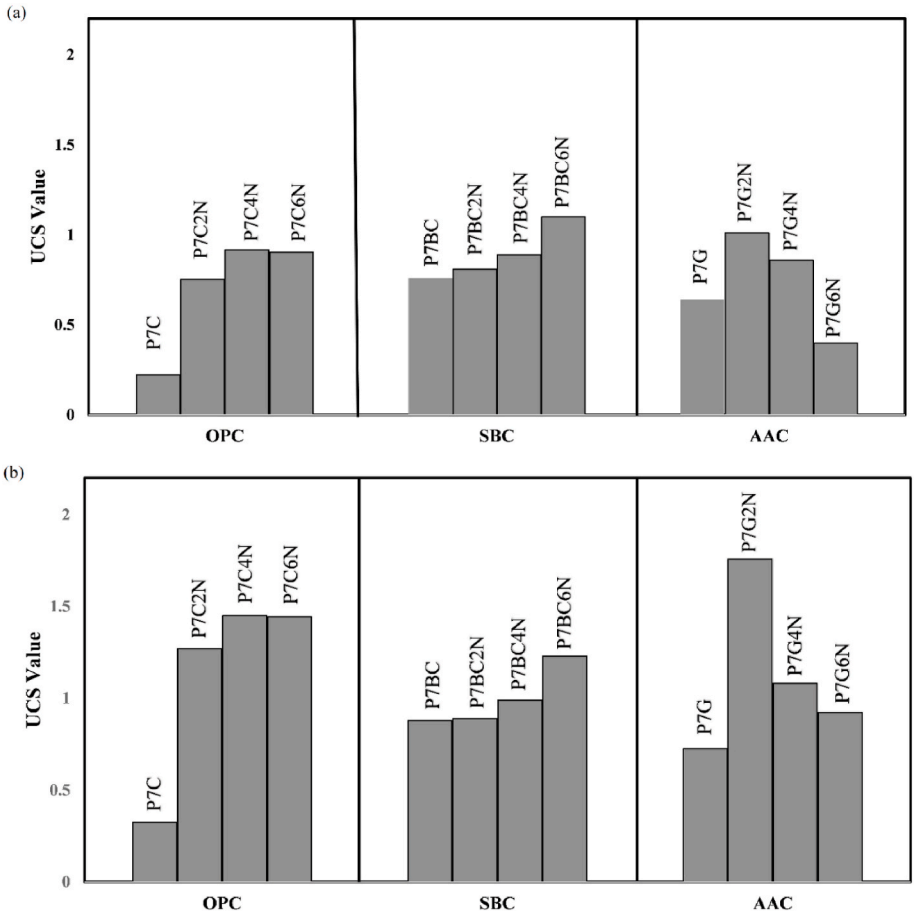

Fig. 5. Compressive strength of stabilized soil by PC, SBC, and AAC in different amounts of Nanosilica 0, 2, 4, and 6 wt% of binders at (a) 28, and (b) 90 days.

addition of Nanosilica for more than 2 wt %, i.e. 4 and 6 wt %, 1.08 MPa and 0.92 MPa for P7G4N and P7G6N after 90 days, respectively. The same trend is also observed for 28-day cured samples. An increase of Nanosilica to 2, 4, and 6 wt % after 90 days of curing improve the UCS value of AAC-based stabilized soil by about 139.73, 47.95, and 26% compared to no added Nanosilica. It seems that higher Nanosilica content, more than 2 wt %, show negative effects on the compressive strength of stabilized soil by AAC. This finding is in agreement with some previous works [26,27], however, in some works Nanosilica with 1 wt%, 2 wt%, and even in some others 3 wt% of Nanosilica has been reported as the optimum value [11,28–30]. In literature, it is also mentioned that at high Nanosilica usage amount, the autogenously shrinkage due to self-desiccation increase and results in a higher cracking potential [24].

3.2. Failure strain

Table 11 represents the failure strain of samples. As seen, the failure strain for the PC-based sample without Nanosilica is 0.93. By adding 2, 4 and 6 wt % of Nanosilica to the mixture, failure strain amounts are increased to 1.25, 1.24, and 1.31% in 90 days of curing, respectively. It seems that adding up to 2 wt % has not a significant effect on failure strain of stabilized samples by PC.

During curing time, an increasing trend is observed for failure strain of pure PC-based sample, from 0.73 to 0.91%. But for samples contained 2, 4, and 6 wt % of Nanosilica the trend is decreasing, i.e. 1.77 to 1.25% for P7C2N, 2.08 to 1.24% for P7C4N, and 2.14 to 1.31% for P7C6N from 28 to 90 days of curing, respectively. The failure strain for the SBC-based sample is 0.83%. By adding 2, 4 and 6 wt% of Nanosilica, the failure strain amounts are increase to 0.85, 0.90, and 1.07% in 90 days of curing, respectively. For SBC-based samples without Nanosilica the failure strain changes from 0.95 to 0.83% in 28 and 90 days of curing, respectively. This amount changes from 1.07 to 0.85% for P7BC2N, 1.07 to 0.9% for P7BC4N, and 1.31 to 1.07% for P7BC6N in the age of 28 and 90 days, respectively. The failure strain for the AAC-based sample is 0.92%. By adding 2, 4 and 6 wt% of Nanosilica, failure strain are increased, but adding Nanosilica from 2 to 4 and 6 wt% shows a descanting trend, 2.89, 2.00, and 1.79% in 90 days of curing, respectively.

For all AAC-based samples, with or without Nanosilica, the failure strain amount increase with curing time. For stabilized sample by AAC without Nanosilica, the failure strain increases from 0.83 to 0.92 in 28 and 90 days, respectively. These amounts increase 1.12–2.89% for P7G2N, 0.97–2.00% for P7G4N, and 0.52–1.79% for P7G6N in the age of 28 and 90 days, respectively.

The above results declare that failure strain in all stabilized samples by different types of binders, i.e. PC, SBC, and AAC, are increased by adding Nanosilica compared to samples without Nanosilica. This may interpret as more ductile behavior when Nanosilica participate in the mixture, however, this point should be consider besides the obtained UCS values and elastic modulus. Now, the main question is that the used Nanosilica to what extend and by how could affect the failure strain in each group of samples with different percentages of Nanosilica. For stabilized samples by PC, there is an increasing trend in strain values by increasing the amount of Nanosilica. However, for samples stabilized by SBC, these amounts are quite similar to each other and a slight increase have been seen. In samples stabilized by AAC a decrease of failure strain has been seen by increasing the amounts of Nanosilica. This could be due to the structural change in the produced AAC sample when Nanosilica is used as an active constituent into activation reaction. This is more discussed in the FTIR test section in continue.

3.3. Elastic modulus

Fig. 6 (a, b, c) demonstrate elastic modulus of samples stabilized by PC, SBC, and AAC, respectively. As seen, the elastic modulus for the PC-based sample is 43.61 MPa. Adding Nanosilica in PC-based samples has an increasing effect on elastic modulus and by adding 2, 4, and 6 wt% of Nanosilica, elastic modulus values are increased to 104.27, 105.35, and 110.57 MPa after 90 days of curing, respectively. Elastic modulus (EM)

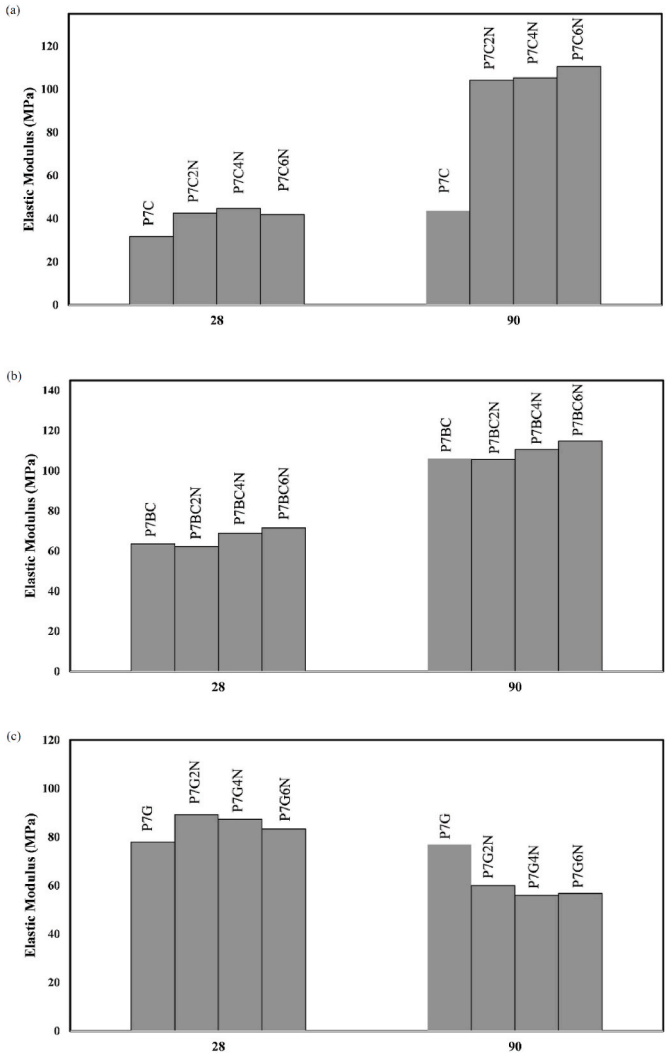

Fig. 6. Elastic Modulus of stabilized soil by (a) PC, (b) SBC, and (c) AAC binders in different amounts of Nanosilica 0, 2, 4, and 6 wt% of binder at 28 days, and 90 days.

Table 11
Failure Strain of stabilized soil by PC, SBC, and AAC binders in different amounts of Nanosilica 0, 2, 4, and 6 wt% of binder at 28 days, and 90 days.

	Failure strain (%)											
	PC				SBC				AAC			
	P7C	P7C2N	P7C4N	P7C6N	P7BC	P7BC2N	P7BC4N	P7BC6N	P7G	P7G2N	P7G4N	P7G6N
28 Days	0.73	1.77	2.08	2.14	0.95	1.07	1.07	1.31	0.83	1.12	0.97	0.52
90 Days	0.91	1.25	1.24	1.31	0.83	0.85	0.90	1.07	0.92	2.89	2.00	1.79

of samples stabilized by pure PC show an increase from 31.64 to 43.61 MPa (with 38% increase) for 28–90 days cured sample. For samples contain 2 wt% of Nanosilica, the EM amount increase from 42.64 to 104.27 MPa (with 144% increase) in the age of 28 and 90 days, respectively. For samples contain 4 wt% of Nanosilica, the EM amount increase from 44.74 to 105.35 MPa (with 135% increase) in the age of 28 and 90 days, respectively. For samples contain 6 wt% of Nanosilica, the EM amount increase from 41.97 to 110.57 MPa (with 163% increase) after 28 and 90 days, respectively. In SBC-based stabilized sample, the elastic modulus is 105.97 MPa. Adding Nanosilica show an increasing trend in elastic modulus and these amounts are 105.52, 110.61, and 114.80 MPa when Nanosilica is added to the mixture in 2, 4, and 6 wt%, respectively.

This trend is valuable for SBC-based samples by increasing curing time, with quite lower increasing rate. For SBC-based samples without added Nanosilica, the elastic modulus increase from 63.54 to 105.97 MPa (with 67% increase) when samples cured from 28 to 90 days, respectively. When Nanosilica is added to mixture in amounts of 2 wt%, the EM values change from 62.23 to 105.52 MPa (with 70% increase) after 28 and 90 days, respectively. For samples contain 4 wt% of Nanosilica, the EM amount increase from 68.92 to 110.61 MPa (with 60% increase) after 28 and 90 days, respectively. For samples contain 6 wt% of Nanosilica, the EM amount increase from 71.59 to 114.80 MPa (with 60% increase) after 28 and 90 days, respectively.

As seen in Fig. 6c, Elastic modulus for stabilized soil by AAC is 76.92 MPa, but the trend is different when Nanosilica treated to the mixture. By adding Nanosilica a decreasing trend can be observed in the elastic modulus values, it seems adding Nanosilica more than 2 wt% has no effect on EM deterioration of AAC-based samples.

Elastic modulus of AAC-based stabilized samples without Nanosilica is quite similar in 28 and 90 days of curing, i.e. 77.93 and 76.92 MPa, respectively. However, when 2 wt% of Nanosilica is added to AAC-based samples, elastic modulus change from 89.29 to 59.96 MPa (with 33% decrease) in 28 and 90 days of curing. For samples contain 4 wt% of Nanosilica, the EM amount decrease from 87.35 to 56.02 MPa (with 36% decrease) in 28 and 90 days of curing. For samples contain 4 wt% of Nanosilica, the EM amount increase from 83.32 to 56.71 MPa (with 32% decrease) after 28 and 90 days.

By considering UCS values in Fig. 5, failure strain in Table 11, and elastic modulus in Fig. 6, since UCS values and failure strain for PC- and SBC-based samples increase by adding and increasing Nanosilica, and also it is observed that the elastic modulus of these samples increase by adding and increasing Nanosilica content in 90-day cured samples, as mentioned before. It could be concluded that the rate of increasing of UCS values are higher than the rate of increasing failure strain in PC- and SBC-based samples. Therefore, by the addition of Nanosilica, samples tend to be more ductile in long term (90 days of curing). Using Nanosilica leads to an increase in UCS and failure strain of all samples for PC- and SBC-based samples. But, the increasing rate of UCS in AAC-based samples are lower than the that of failure strain that seems adding Nanosilica in AAC-based samples tend them to be more ductile specially in the long term of curing (after 90 days of curing). On the other hand, by increasing Nanosilica for more than 2 wt% in AAC-based samples, UCS values and failure strain decreased. Also, the elastic modulus results show that the increasing Nanosilica decrease the elastic modulus in 90 days cured samples. It means that by increasing Nanosilica, the decreasing rate of UCS values are higher than the decreasing rate of failure strain in AAC-based samples that proved the higher tendency of more ductile products (after 90 days of curing).

3.4. Binder analysis

3.4.1. X-ray diffraction

X-ray diffraction analysis is performed to establish a suitable

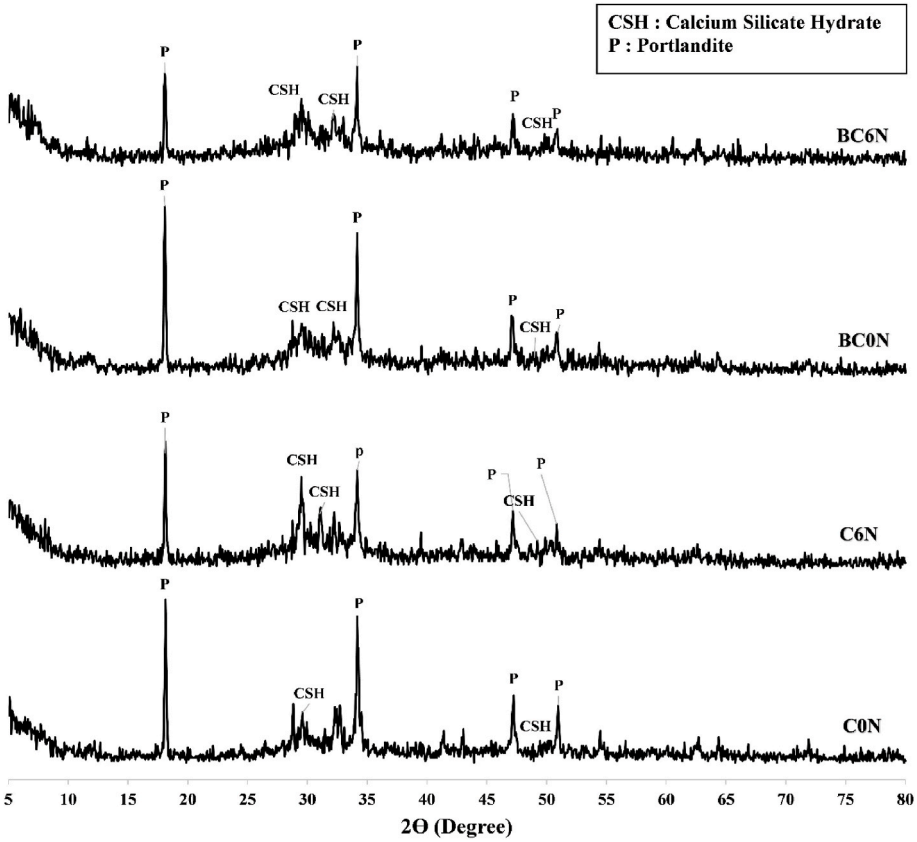

Fig. 7. XRD patterns for C0N, C6N, BC0N, and BC6N.

criterion for investigation of the crystalline phases of the used Portland cement and blended cement binders in UCS test. The main aim of this test is to understand the effect of Nanosilica in the chemical activity of the binder mixtures and its probable effect on crystalline structure. Fig. 7 presents the XRD patterns of C0N, C6N, BC0N, and BC6N after 90 days of curing. These binders have been used for P7C, P7C6N, P7BC0N, and P7BC6N samples in UCS test, respectively. As seen, Calcium-silicate-hydrate (C–S–H; JCDPS 33–0306) and Portlandite ($Ca(OH)_2$; JCPDS 44–1481) are observed in Fig. 7. As seen in Fig. 7, the main hydration product of phosphorus slag-blended cement is similar to that of PC, which is C–S–H. It seems that Nanosilica has an effect on intensifying Calcium-silicate-hydrate (C–S–H; JCDPS 33–0306) when C6N and BC6N are compared to C0N and BC0N in Fig. 7. Also, it is mentioned that Nanosilica incorporated samples show a decrease in the intensify of Portlandite ($Ca(OH)_2$; JCPDS 44–1481) compared to non-incorporated samples. The reason for this phenomenon could be due to consuming calcium hydroxid by Nanosilica particles and creating more C–S–H gel [20,21,31].

It can be concluded that the interring reactive silica to the matrix from the source of Nanosilica can help the better participation reaction of Ca^{2+} of Portlandite to formation of more C–S–H crystalline phase that mainly result in higher strength.

3.4.2. FTIR

The activation process for formation of alkali-activated materials, namely dissolution, orientation, and polycondensation, leads amorphous structure of raw material to a new semi-crystaline structure. So, it seems better to apply FTIR technique for studying the molecular structure [32].

In this study, FTIR spectroscopy method is used for bond structures investigation of AAC0N and AAC2N which are the binders of P7G and P7G2N samples, and this samples are tested after 90 days of curing. Fig. 8 depicts the FTIR spectra of alkali-activated phosphorus slag binder without or with presence of 2 wt% of Nanosilica.

The bands in the range of 450 cm^{-1} and 1000 cm^{-1} wavenumber are related to Si–O–Al and silicate chain bonds [33–35]. Also, there are some bands attributable to stretching and bending vibrations of OH groups in the wavenumbers of 1650 cm^{-1} and 3500 cm^{-1} [32,36].

In AAC2N, the bands in the range of 450–500 cm−1 become sharp with less intensity confirming more formation of Si–O–Al bonds in AAC0N. For AAC0N, the bands in the range of 1000 cm−1 show stronger and sharper peak that indicate the presence of Nanosilica with an effect on alleviating the intensifying of spectra.

As seen in Fig. 8, the main peak in the range of 960 cm^{-1} for AAC0N which is the non-incorporated Nanosilica binder shifted to wavenumbers of 970 cm^{-1} for Nanosilica incorporated binder, i.e. AAC2N. This could be due to structural effect of Nanosilica on lengthening the Si–O–Si and Si–O–Al chain in the matrix. Samples with higher amounts of Nanosilica (more than 2 wt%) have this structural change with long Si–O–Si and Si–O–Al chain in the matrix. This phenomena can result in a decrease in mechanical strength of the final product [37]. This is in line with the observed decrease in failure strength in activated slag with more than 2 wt% of Nanosilica.

3.5. Microstructural assessment

The SEM/EDS analysis revealed some noteworthy points in terms of the microstructure of the matrix of studied binders and also the addition of Nanosilica to the binders. The SEM/EDS is applied to stabilized soil samples in different magnifications of 500, 1500, and 5000x for P7C, P7C6N, P7BC, P7BC6N, P7G, P7G2N, and P7G6N samples. Furthermore, the magnification of 10000x is applied for P7C6N, P7BC6N, P7G2N, and P7G6N, the ones which contained Nanosilica.

Fig. 9 shows the SEM images of 90-day cured of P7C (without Nanosilica) and P7C6N (with 6 wt% of Nanosilica). As seen in Fig. 9 (a, c), presence of Nanosilica has a profound effect on microstructural modification and also densification of binders, so that, more coverage of soil particles is observed in the sample containing Nanosilica that results in higher UCS values and elastic modulus (observed in Figs. 5 and 6).

Table 12 presents the EDS done on points A and B in Fig. 9 which are the matrix of the used binders of PC and PC containing Nanosilica. As was expected the measured Si element in the matrix is increased with addition of Nanosilica. As mentioned in the XRD test (Fig. 7), more C–S–H phase is observed in the Nanosilica containing matrix which could be proved with the more measured Si in the elemental analysis that incorporated in the formation of more C–S–H phase. This could also be observed in the phase change of needle-like crystals of Portlandite in Fig. 9b to lower amount with smaller particles in Fig. 9d in the presence Nanosilica.

Fig. 10 depicts the SEM images of 90-day cured of P7BC (without Nanosilica) and P7BC6N (with 6 wt% of Nanosilica). As seen in Fig. 10 (a, c), presence of Nanosilica has a profound effect on microstructural modification and also densification of binders, so that, more coverage of soil particles is observed in the sample containing Nanosilica that results

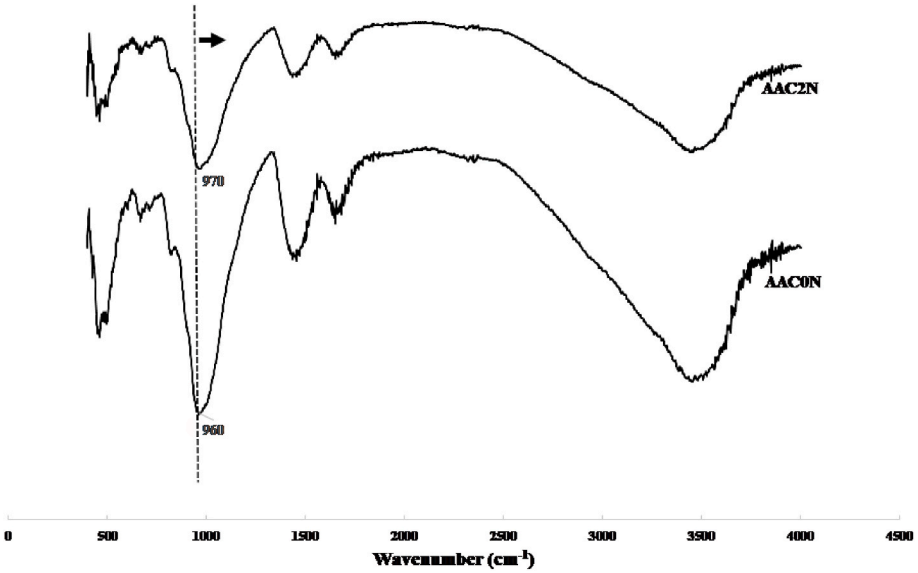

Fig. 8. FTIR spectra of AAC0N and AAC2N binders.

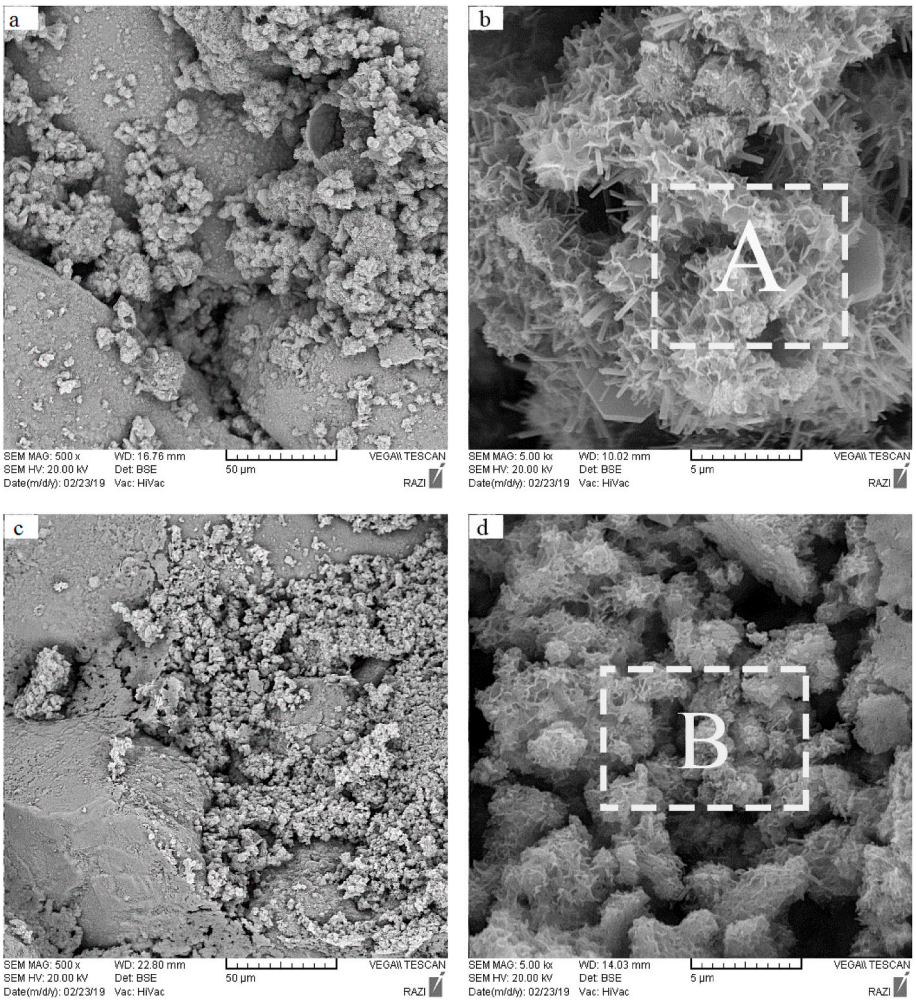

Fig. 9. SEM images of 90-day cured P7C (a,b) and P7C6N (c, d) in magnifications of 500x and 5000x

Table 12
Elemental Analysis done on point A and B shown in Fig. 9

Element (wt.%)	O	Mg	Al	Si	Ca	K	Fe
Point A	57.71	3.13	1.92	7.61	25.71	0.86	3.07
Point B	55.99	0.67	1.74	13.24	25.24	1.38	1.74

in slightly higher UCS values and elastic modulus (observed in Figs. 5 and 6).

As seen in Fig. 10b, a number of unreacted particles of phosphorus slag could be observed which are markedly decreased in Fig. 10d. This could be due to the progress of hydration reaction of phosphorus slag and Portland cement in presence of Nanosilica as an active filler that results in the consumption of needle-like Portlandite phase to have more C–S–H in the matrix (as seen in Fig. 7 BCE0N and BC6N).

Table 13 presents the EDS done on points A and B in Fig. 10 which are the matrix of the used binders of SBC and SBC containing Nanosilica. P7BC6N presents slightly more C–S–H phase compared to P7BC in Fig. 7. This result can be observed in the UCS values in Fig. 5 and also in XRD analysis which P7BC6N presents C–S–H with quite similar intensity.

Comparing Fig.s. 10c and c results in more densified matrix for PC containing samples with the soil particles. The higher UCS values for P7C6N compared to P7BC6N could be due to its more densified ITZ.

As seen in Fig. 11 (a, c, and e), the sample P7G2N containing 2 wt% of Nanosilica shows more densified ITZ with strong bond between the matrix and soil particles compared to P7G and P7G6N. This can be the results of higher strength in the mentioned samples compared to the others. This sows that an optimum usage of Nanosilica is necessary in the activated phosphorus slag to obtain higher UCS values. This could be due to the structural effect of Nanosilica, as mentioned in FTIR test in Fig. 8. The excessive amount of Nanosilica (more than 2 wt%), in samples results in lower UCS values with relatively loose interlocking morphology with higher amount of open pores in the binder.

Table 14 presents the EDS done on points A, B, and C in Fig. 11 which are the matrix of the used binders of AAC and AAC containing Nanosilica. As seen in Table 14, the measured Si element in the matrix is increased with addition of Nanosilica. Due to elemental analysis of raw phosphorus slag shown in Table 5, the presented calcium ion (Ca^{+2}) and sulfur ion (S^{-2}) in Table 14 could be the result of leaching out of these ions from activated phosphorous slag [10].

4. Conclusions

The key findings in this study can be summarized with the following conclusive statements:

1. PC- and SBC-based stabilized soil samples containing Nanosilica showed an increase in the UCS values. The UCS value for PC-based samples seems to be constant with addition of Nanosilica for more than 4 wt%. This could be due to chemical reactivity of pozzolanic activity of Nanosilica and its potential acceleration effect in Portland cement and blended cement. Nanosilica's participation in the hydration can lead to nucleation site for precipitation of C–S–H gel. In

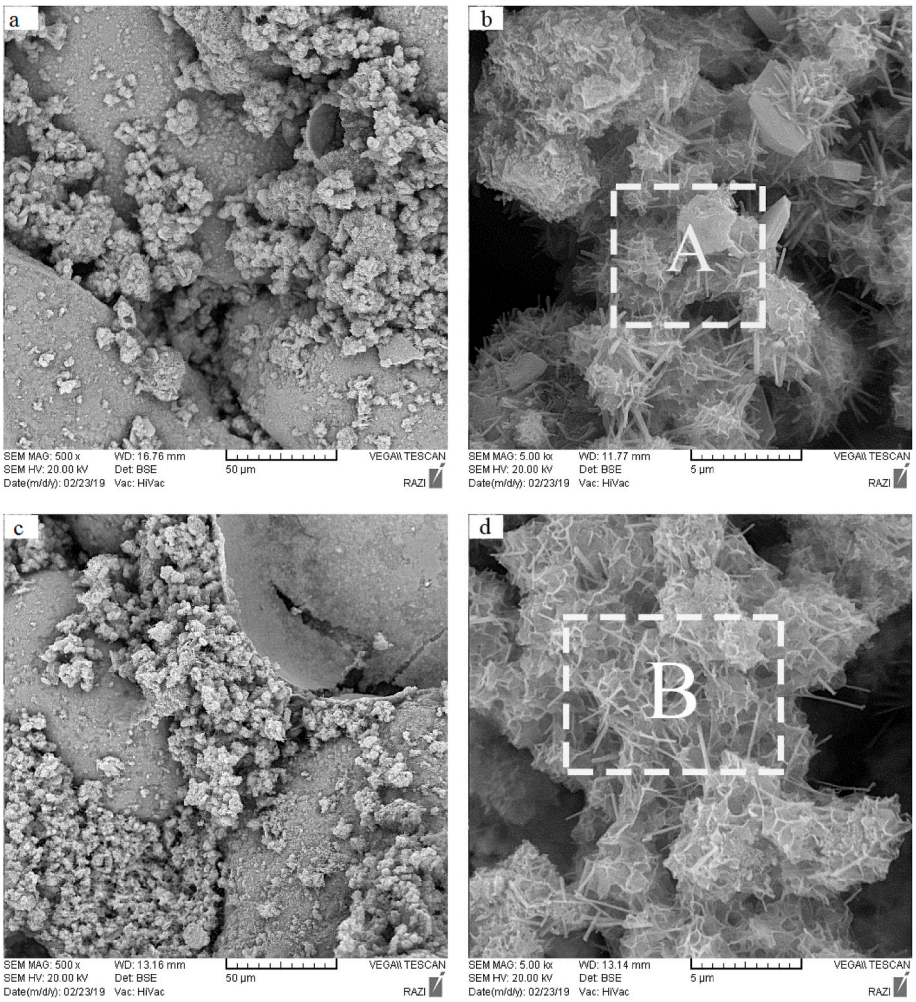

Fig. 10. SEM images of 90-day cured P7BC (a,b) and P7BC6N (c, d) in magnifications of 500x and 5000x

Table 13
Elemental Analysis done on point A and B shown in Fig. 10

Element (wt. %)	O	Mg	Al	Si	Ca	K	Fe	S
Point A	50.91	0.94	3.74	10.69	25.57	0.71	3.05	4.40
Point B	53.57	–	1.71	11.74	30.96	0.83	1.19	–

AAC-based samples, the optimum dosage amount of Nanosilica is found to be 2 wt% according to UCS test. The observed negative effect of high Nanosilica dosage on the compressive strength of stabilized soil by AAC could be due to autogenous shrinkage increase of self-desiccation which results in a higher cracking potential in the matrix that leads to reduction in UCS values. Excessive amount of Nanosilica (more than 2 wt%) results in lower UCS values with relatively loose interlocking morphology with higher amount of open pores in the binder.

2. By comparing the obtained UCS values and failure strains, it could be concluded that the used cementing materials, have high tendency for producing more ductile samples when incorporated with Nanosilica. This characteristic would be beneficial in many civil engineering applications where ductile materials are needed. However, economical issues should be taken into account so that adding Nanosilica may not be a practical option at current situation in some projects depending on its cost and availability.
3. The main hydration product of phosphorus slag-blended cement is similar to that of PC, i.e. C–S–H and Portlandite phases. Samples containing Nanosilica showed an intensified C–S–H compared to non-involving samples. Moreover, supplying reactive silica to the matrix from the Nanosilica showed better participation reaction of Ca^{2+} of Portlandite to formation of more C–S–H crystalline phase that potentially results in higher strength.
4. In the alkali-activated slag containing 2 wt% of Nanosilica compared to non-incorporated Nanosilica binder, a shift is observed from 960 cm^{-1} to wavenumbers of 970 cm-1 in the FTIR spectrums which could be due to structural effects of Nanosilica on lengthening the Si–O–Si and Si–O–Al chains in the matrix. It seems that Al is substituted by reactive entering Si from Nanosilica. This could be a proof for the observed decrease in failure strength by increasing the amount of Nanosilica in activated slag for more than 2 wt%.
5. Presence of Nanosilica as a reactive powder has a profound effect on microstructural modification and also densification of binders with more coverage of soil particles and higher progress of hydration reaction of phosphorus slag and Portland cement with more consumption of unreacted phosphorus slag. Additionaly, the measured Si element in the matrix increases with the addition of Nanosilica. This could be incorporated in the formation of more C–S–H phase. A phase change of needle-like crystals of Portlandite to a lower amount with smaller particles in the Nanosilica containing samples was observed which could lead to more C–S–H in the matrix.

Credit author statement

Ebrahim Najafi Kani: Data curation, Methodology; Validation,

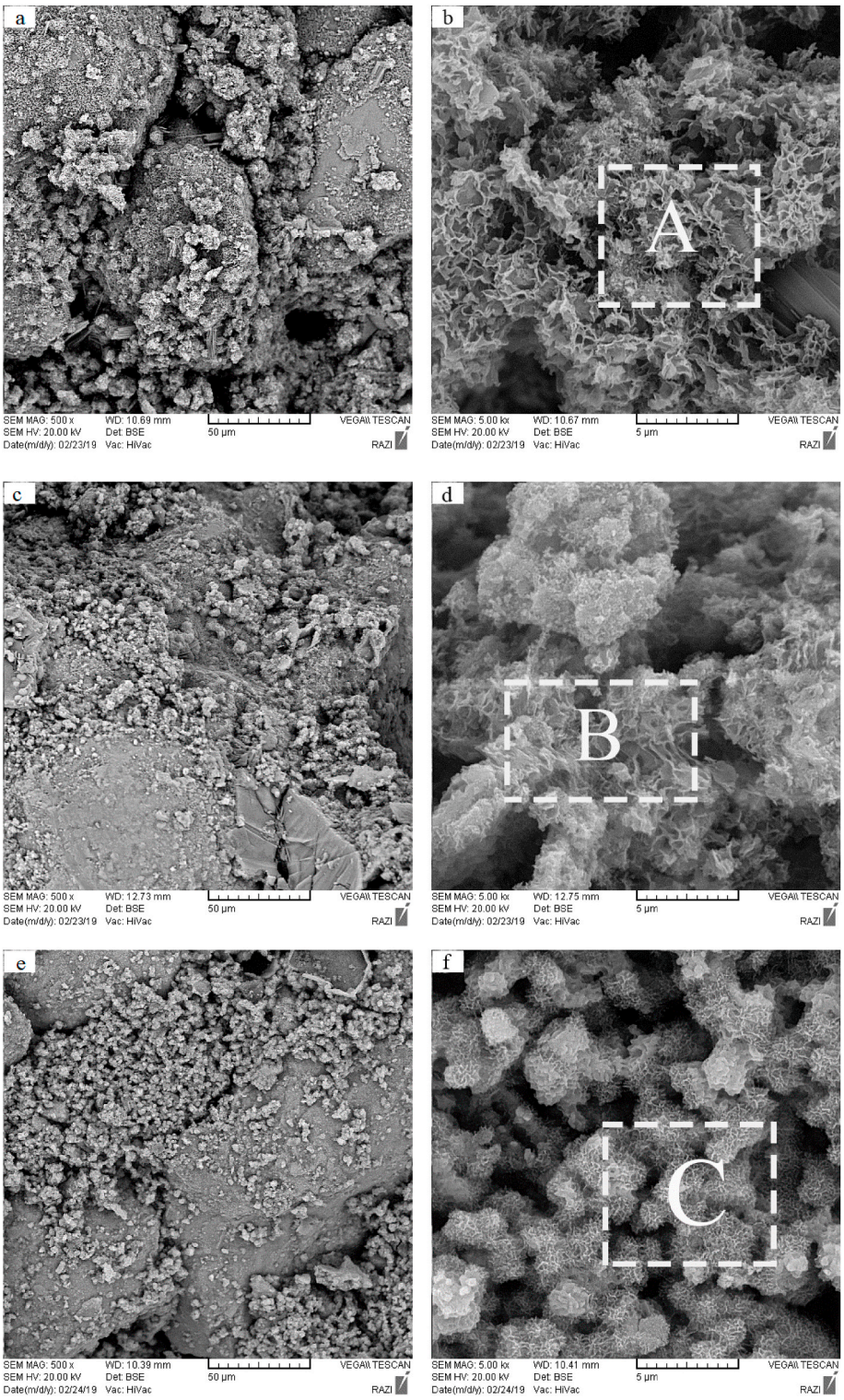

Fig. 11. SEM images of 90-day cured P7G (a,b), P7G2N (c, d), and P7G6N (e, f) in magnifications of 500x and 5000x

Table 14
Elemental Analysis done on point A, B, and C shown in Fig. 11

Element (wt. %)	O	Al	Si	Ca	K	Fe	S	Na
Point A	55.79	1.62	12.19	17.44	0.29	0.75	6.61	5.30
Point B	55.45	2.47	14.62	15.90	0.20	1.31	3.55	5.16
Point C	51.70	2.15	17.03	21.84	0.65	0.76	2.75	3.11

Investigation, Writing - Original Draft, Visualization, Supervision. Amir Hossein Rafiean: Data curation, Methodology; Validation, Writing - Review & Editing. Mohsen Tavakolzadeh: Data curation, Methodology; Validation, Writing - Review & Editing. Seyed Hamidreza Ghaffar: Writing - review & editing, Resources, Writing - Original Draft, Visualization, Supervision.

Declaration of competing interest

The authors declare that they have no known competing financial interests or personal relationships that could have appeared to influence the work reported in this paper.

Data availability

Data will be made available on request.

References

[1] T. Santos, J. Almeida, J.D. Silvestre, P. Faria, Life cycle assessment of mortars: a review on technical potential and drawbacks, Construct. Build. Mater. 288 (2021), 123069, https://doi.org/10.1016/j.conbuildmat.2021.123069.

[2] A. Behnood, Soil and clay stabilization with calcium- and non-calcium-based additives : a state-of-the-art review of challenges , approaches and techniques, Transp. Geotech. (2018), https://doi.org/10.1016/j.trgeo.2018.08.002.

[3] J.K. Mitchell, Behavior Jk Mitchell Amp K Soga Fundamentals of Soil Behavior, 2005.

[4] S.H. Ghaffar, M. Al-Kheetan, P. Ewens, T. Wang, J. Zhuang, Investigation of the interfacial bonding between flax/wool twine and various cementitious matrices in mortar composites, Construct. Build. Mater. 239 (2020), 117833, https://doi.org/10.1016/j.conbuildmat.2019.117833.

[5] M. Chougan, S.H. Ghaffar, P. Sikora, S.Y. Chung, T. Rucinska, D. Stephan, A. Albar, M.R. Swash, Investigation of additive incorporation on rheological, microstructural and mechanical properties of 3D printable alkali-activated materials, Mater. Des. 202 (2021), https://doi.org/10.1016/j.matdes.2021.109574.

[6] D. Rezazadeh Eidgahee, A.H. Rafiean, A. Haddad, A novel formulation for the compressive strength of IBP-based geopolymer stabilized clayey soils using ANN and GMDH-NN approaches, Iran, J. Sci. Technol. Trans. Civ. Eng. (2019), https://doi.org/10.1007/s40996-019-00263-1.

[7] A. Hossein Rafiean, E. Najafi Kani, A. Haddad, Mechanical and durability properties of poorly graded sandy soil stabilized with activated slag, J. Mater. Civ. Eng. 32 (2020), 04019324, https://doi.org/10.1061/(ASCE)MT.1943-5533.0002990.

[8] K. Liu, Y. Cui, Effects of different content of phosphorus slag composite concrete: heat evolution, sulphate-corrosion resistance and volume deformation, Crystals 11 (2021) 1293, https://doi.org/10.3390/cryst11111293.

[9] H. Mehdizadeh, E. Najafi Kani, A. Palomo Sanchez, A. Fernandez-Jimenez, Rheology of activated phosphorus slag with lime and alkaline salts, Cement Concr. Res. 113 (2018) 121–129, https://doi.org/10.1016/j.cemconres.2018.07.010.

[10] H. Mehdizadeh, E. Najafi Kani, Rheology and apparent activation energy of alkali activated phosphorous slag, Construct. Build. Mater. 171 (2018) 197–204, https://doi.org/10.1016/j.conbuildmat.2018.03.130.

[11] A.A. Raheem, R. Abdulwahab, M.A. Kareem, Incorporation of metakaolin and nanosilica in blended cement mortar and concrete- A review, J. Clean. Prod. 290 (2021), 125852, https://doi.org/10.1016/j.jclepro.2021.125852.

[12] P. Sargent, The Development of Alkali-Activated Mixtures for Soil Stabilisation, Woodhead Publishing Limited, 2015, https://doi.org/10.1533/9781782422884.4.555.

[13] Z.S. Metaxa, A.K. Tolkou, S. Efstathiou, A. Rahdar, E.P. Favvas, A.C. Mitropoulos, G.Z. Kyzas, Nanomaterials in cementitious composites: an update, Molecules 26 (2021) 1430, https://doi.org/10.3390/molecules26051430.

[14] E. Najafi Kani, A.H. Rafiean, A. Alishah, S. Hojjati Astani, S.H. Ghaffar, The effects of Nano-Fe2O3 on the mechanical, physical and microstructure of cementitious composites, Construct. Build. Mater. 266 (2021), 121137, https://doi.org/10.1016/j.conbuildmat.2020.121137.

[15] E.U. Eyo, S. Ng'ambi, S.J. Abbey, Incorporation of a nanotechnology-based additive in cementitious products for clay stabilisation, J. Rock Mech. Geotech. Eng. 12 (2020) 1056–1069, https://doi.org/10.1016/j.jrmge.2019.12.018.

[16] M. Chougan, E. Marotta, F.R. Lamastra, F. Vivio, G. Montesperelli, U. Ianniruberto, S. Hamidreza Ghaffar, M.J. Al-kheetan, A. Bianco, High performance cementitious nanocomposites: the effectiveness of nano-Graphite (nG), Construct. Build. Mater. 259 (2020), https://doi.org/10.1016/j.conbuildmat.2020.119687, 119687.

[17] F.R. Lamastra, M. Chougan, E. Marotta, S. Ciattini, S.H. Ghaffar, S. Caporali, F. Vivio, G. Montesperelli, U. Ianniruberto, M.J. Al-Kheetan, A. Bianco, Toward a better understanding of multifunctional cement-based materials: the impact of graphite nanoplatelets (GNPs), Ceram. Int. 47 (2021), https://doi.org/10.1016/j.ceramint.2021.04.012, 20019–20031.

[18] S.H. Bahmani, N. Farzadnia, A. Asadi, B.B.K. Huat, The effect of size and replacement content of nanosilica on strength development of cement treated residual soil, Construct. Build. Mater. 118 (2016) 294–306, https://doi.org/10.1016/j.conbuildmat.2016.05.075.

[19] D. Kong, X. Du, S. Wei, H. Zhang, Y. Yang, S.P. Shah, Influence of nano-silica agglomeration on microstructure and properties of the hardened cement-based materials, Construct. Build. Mater. 37 (2012) 707–715, https://doi.org/10.1016/j.conbuildmat.2012.08.006.

[20] J. Wang, Y. Cheng, L. Yuan, D. Xu, P. Du, P. Hou, Z. Zhou, X. Cheng, S. Liu, Y. Wang, Effect of nano-silica on chemical and volume shrinkage of cement-based composites, Construct. Build. Mater. 247 (2020), 118529, https://doi.org/10.1016/j.conbuildmat.2020.118529.

[21] G.C. Isaia, A.L.G. Gastaldini, R. Moraes, Physical and pozzolanic action of mineral additions on the mechanical strength of high-performance concrete, Cem. Concr. Compos. 25 (2003) 69–76, https://doi.org/10.1016/S0958-9465(01)00057-9.

[22] L. Senff, D. Hotza, W.L. Repette, V.M. Ferreira, J.A. Labrincha, Mortars with nano-SiO2 and micro-SiO2 investigated by experimental design, Construct. Build. Mater. 24 (2010) 1432–1437, https://doi.org/10.1016/j.conbuildmat.2010.01.012.

[23] L. Senff, J.A. Labrincha, V.M. Ferreira, D. Hotza, W.L. Repette, Effect of nano-silica on rheology and fresh properties of cement pastes and mortars, Construct. Build. Mater. 23 (2009) 2487–2491, https://doi.org/10.1016/j.conbuildmat.2009.02.005.

[24] G. Quercia, G. Hüsken, H.J.H. Brouwers, Water demand of amorphous nano silica and its impact on the workability of cement paste, Cement Concr. Res. 42 (2012) 344–357, https://doi.org/10.1016/j.cemconres.2011.10.008.

[25] Y. Qing, Z. Zenan, K. Deyu, C. Rongshen, Influence of nano-SiO2 addition on properties of hardened cement paste as compared with silica fume, Construct. Build. Mater. 21 (2007) 539–545, https://doi.org/10.1016/j.conbuildmat.2005.09.001.

[26] K.W. Lo, K.L. Lin, T.W. Cheng, Y.M. Chang, J.Y. Lan, Effect of nano-SiO2 on the alkali-activated characteristics of spent catalyst metakaolin-based geopolymers, Construct. Build. Mater. 143 (2017) 455–463, https://doi.org/10.1016/j.conbuildmat.2017.03.152.

[27] P.S. Deb, P.K. Sarker, S. Barbhuiya, Sorptivity and acid resistance of ambient-cured geopolymer mortars containing nano-silica, Cem. Concr. Compos. 72 (2016) 235–245, https://doi.org/10.1016/j.cemconcomp.2016.06.017.

[28] X. Gao, Q.L. Yu, H.J.H. Brouwers, Characterization of alkali activated slag-fly ash blends containing nano-silica, Construct. Build. Mater. 98 (2015) 397–406, https://doi.org/10.1016/j.conbuildmat.2015.08.086.

[29] Y. Zhou, S. Zheng, X. Huang, B. Xi, Z. Huang, M. Guo, Performance enhancement of green high-ductility engineered cementitious composites by nano-silica incorporation, Construct. Build. Mater. 281 (2021), 122618, https://doi.org/10.1016/j.conbuildmat.2021.122618.

[30] W. Li, Z. Huang, F. Cao, Z. Sun, S.P. Shah, Effects of nano-silica and nano-limestone on flowability and mechanical properties of ultra-high-performance concrete matrix, Construct. Build. Mater. 95 (2015) 366–374, https://doi.org/10.1016/j.conbuildmat.2015.05.137.

[31] D. da Silva Andrade, J.H. da Silva Rêgo, P.C. Morais, A.N. de Mendonça Lopes, M. F. Rojas, Investigation of C-S-H in ternary cement pastes containing nanosilica and highly-reactive supplementary cementitious materials (SCMs): microstructure and strength, Construct. Build. Mater. 198 (2019) 445–455, https://doi.org/10.1016/j.conbuildmat.2018.10.235.

[32] H. Mehdizadeh, E. Najafi Kani, A. Palomo Sanchez, A. Fernandez-Jimenez, Rheology of activated phosphorus slag with lime and alkaline salts, Cement Concr. Res. 113 (2018) 121–129, https://doi.org/10.1016/j.cemconres.2018.07.010.

[33] A.R. Sakulich, E. Anderson, C. Schauer, M.W. Barsoum, Mechanical and microstructural characterization of an alkali-activated slag/limestone fine aggregate concrete, Construct. Build. Mater. 23 (2009) 2951–2957, https://doi.org/10.1016/j.conbuildmat.2009.02.022.

[34] F. Puertas, M. Palacios, H. Manzano, J.S. Dolado, A. Rico, J. Rodríguez, A model for the C-A-S-H gel formed in alkali-activated slag cements, J. Eur. Ceram. Soc. 31 (2011) 2043–2056, https://doi.org/10.1016/j.jeurceramsoc.2011.04.036.

[35] A. Allahverdi, E. Najafi Kani, B. Shaverdi, Carbonation versus efflorescence in alkali-activated blast-furnace slag in relation with chemical composition of activator, Int. J. Civ. Eng. 15 (2017) 565–573, https://doi.org/10.1007/s40999-017-0225-4.

[36] E.N. Kani, A. Allahverdi, Effects of curing time and temperature on strength development of inorganic polymeric binder based on natural pozzolan, J. Mater. Sci. 44 (2009) 3088–3097, https://doi.org/10.1007/s10853-009-3411-1.

[37] E. Najafi Kani, A. Allahverdi, J.L. Provis, Efflorescence control in geopolymer binders based on natural pozzolan, Cem. Concr. Compos. 34 (2012) 25–33, https://doi.org/10.1016/j.cemconcomp.2011.07.007.